Journal of Systems Engineering and Electronics
Vol. PP, No. 99, November 2022, pp.1 – 13

Triad-displaced ULAs configuration for non-circular sources with larger continuous virtual aperture and enhanced degrees of freedom

SHAIKH Abdul Hayee *, DANG Xiaoyu, and HUANG Daqing

College of Electronic and Information Engineering, Nanjing University of Aeronautics and Astronautics, Nanjing 211106, China

Abstract: Non-uniform linear array (NULA) configurations are well renowned due to their structural ability for providing increased degrees of freedom (DOF) and wider array aperture than uniform linear arrays (ULAs). These characteristics play a significant role in improving the direction-of-arrival (DOA) estimation accuracy. However, most of the existing NULA geometries are primarily applicable to circular sources (CSs), while they limitedly improve the DOF and continuous virtual aperture for non-circular sources (NCSs). Toward this purpose, we present a triad-displaced ULAs (Tdis-ULAs) configuration for NCS. The Tdis-ULAs structure generally consists of three ULAs, which are appropriately placed. The proposed antenna array approach fully exploits the non-circular characteristics of the sources. Given the same number of elements, the Tdis-ULAs design achieves more DOF and larger hole-free co-array aperture than its sparse array competitors. Advantageously, the number of uniform DOF, optimal distribution of elements among the ULAs, and precise element positions are uniquely determined by the closed-form expressions. Moreover, the proposed array also produces a filled resulting co-array. Numerical simulations are conducted to show the performance advantages of the proposed Tdis-ULAs configuration over its counterpart designs.

Keywords: direction-of-arrival (DOA) estimation, sparse array, non-circular source (NCS), sum co-array, difference co-array, degrees of freedom (DOF).

DOI: 10.23919/JSEE.2022.000128

1. Introduction

Over the years, direction-of-arrival (DOA) estimation has remained one of the critical issues for array signal processing, which finds traces in various communication fields [1−4]. The sensor arrays perform spatial sampling of incident source signals, and the key benefits of utilizing them include enhancing the signal quality, mitigating interference, and spatial selectivity. Traditionally, the uniform linear arrays (ULAs) are employed as sensor arrays to resolve $N-1$ sources for the N number of antennas, using the subspace-based DOA estimation methods [5−7]. The achievable degrees of freedom (DOF) for ULAs can only be improved at the expense of additional elements, thereby increasing the overall hardware cost and complexity [8]. Hence, the ULAs are not suitable for under-determined conditions where the number of impinging sources is higher than physical antennas [9,10]. Moreover, ULAs are constructed with a unit inter-sensor spacing, leading to severe mutual coupling effects between the antennas.

The construction of ULAs (NULAs), commonly known as sparse arrays, presents a promising solution to these challenges [11]. The sparse array geometries dramatically increase the DOF and reduce the mutual coupling effects by maintaining a wider inter-sensor spacing compared to the ULAs [12,13]. In this regard, the minimum redundancy array is among the most renowned NULA designs that can achieve a higher number of DOF with a larger array aperture [14,15]. Although these arrays maximize the achievable DOF, the lack of closed-form expressions for DOF and array geometry restricts their systematic design. Hence the optimum configuration of minimum redundancy arrays is difficult, and in most cases, it requires complicated algorithms, which leads to computational burden [16].

On the other hand, several NULA geometries, such as nested array (NA) [17,18], co-prime array [19,20], super NA [21], improved NA (INA) [22], are introduced as attractive alternatives. Unlike non-redundant arrays, all of these configurations formulate closed-form expressions to determine the achievable DOF and physical sensor positions. Hence, implementing such configurations

Manuscript received September 22, 2021.
*Corresponding author.
This work was supported by the National Natural Science Foundation of China (62031017;61971221) and the Fundamental Research Funds for the Central Universities of China (NP2020104).

becomes easy and systematic; meanwhile, they can provide more DOF than ULAs. The NA [18] is designed by effectively combining a dense ULA with a sparse ULA to handle more source signals than the number of antennas. Although the NA [18] benefits from closed-form expressions, they offer fewer DOF than minimum redundancy arrays. While half of the total physical sensors for the NA are placed in the ULA with a unit inter-sensor spacing; thus, the NA [18] also remains sensitive to mutual coupling leakage [23]. In order to overcome the disadvantage of the NA [18], the super NA is introduced [21], which attains the same hole-free co-array aperture as the NA [18]. However, the super NA [21] are less prone to coupling effects than NA [18]. To further enhance the DOF, the extension of the NA [18] known as INA was introduced [22]. The INA [22] geometry can provide a wider continuous virtual aperture and a higher DOF capacity. In [24], an augmented approach for the NA was examined, which splits the compact ULA of the NA into sparse ULAs and positions them on the sides of the NA [18] to achieve more DOF and virtual aperture than the original NA [18]. Recently, the construction of an enhanced NA has been demonstrated in [25], which concatenates dense and sparse ULA with a separate sensor placed between them. However, it can increase only two DOFs compared to NA [18], which is only valid when the given number of sensors is even.

The co-prime design is another fascinating NULA configuration, which uses a co-prime pair of uniform linear sub-arrays [19]. This array designing methodology significantly reduces the mutual coupling effects. Nonetheless, for a fixed number of elements, the uniform DOF (uDOF) offered by NA [18] is higher than the co-prime array [19], and the resulting co-array of co-prime is also filled with some holes, which may compromise the DOA estimation accuracy. In [26], an extended co-prime design was proposed, which achieves more DOF and better DOA estimation accuracy than the prototype co-prime [19] by doubling the number of elements in one subarray. To further improve the DOA estimation performance of a co-prime structure, the concept of array interpolation [27,28] is introduced, which makes full use of all the virtual sensors in its co-array. In [29], a new co-prime structure is constructed by translocating one subarray of a co-prime design and rotating the axis with a compressed inter-element spacing of the second subarray, which obtains more DOF in co-array. However, its implementation requires the number of elements in one subarray set to be an even number greater than two.

Later, the maximum inter-element spacing constraint (MISC) arrays were introduced in [30]. Compared to nested and co-prime counterparts, it achieves more DOF with an extended virtual aperture. However, the realization of MISC arrays requires at least five elements. In [31], a three-stage padding configuration for the sparse arrays was presented, which cascades three identical subarrays to configure a sparse structure that can provide more DOF and a wider continuous virtual aperture. A pentad-displaced ULAs design based on five ULAs and a single sensor was recently presented [32]. This sensor array achieves more DOF and a larger hole-free virtual array than its existing competitors. Nevertheless, designing this sparse structure is possible with at least eight physical sensors.

Notably, all the NULA structures mentioned above are mainly designed to resolve the circular sources (CS). However, many non-circular sources (NCSs) exist practically [33,34]. The NCS contain more information than its circular counterparts. Importantly, the elliptic covariance of CS is zero, while the NCS have a non-zero value for elliptic covariance that can be exploited to enlarge the co-array aperture and increase the DOF. Different DOA estimation methods are proposed for NCS [35,36]. However, these methods either utilize the ULAs [35] or sparse structures [36] originally designed from a difference coarray perspective. Hence, due to their structural limitations, the non-zero elliptic covariance property, through which a sum co-array can be additionally obtained, is not sufficiently utilized. As a result, the characteristics of NCS are not fully exploited, especially from the array designing perspective, which greatly fascinates the researchers to work on this issue in recent times.

In order to meet such an objective, more judicious placement of sensors in the physical array is desirable, which can make the joint use of the sum and difference co-array more effective to enlarge the continuous virtual aperture and increase the DOF. Toward this purpose, the NA with displaced subarray (NADiS) [37] configuration is introduced for NCS. By enlarging the inter-sensor spacing of the sparse ULA and redefining the displacement between the two ULAs of the NA [18], the NADiS [37] shows a significant increase in the DOF and virtual aperture for NCS. Nevertheless, its resulting co-array is not hole-free. In [38], a new NA (NNA) was presented for jointly utilizing the sum and difference coarray, which can obtain more DOF than the prototype NA [18]. However, this design lacks implementation for an odd number of sensors. A novel sparse array for NCS (SANCS) was designed for the DOA estimation of NCS [39], which offers more DOF than the aforementioned sparse arrays. However, the physical locations in the SANCS array are determined through an exhaustive search algorithm. Thus designing the SANCS array becomes a herculean task due to the unavailability of closed-form expressions for antenna placement and uDOF. Besides, its resulting co-

array also contains holes. A new SANCS (NSANCS) [40] benefiting from closed-form expressions was recently introduced to obtain a hole-free resulting ULA with a higher DOF capacity for NCS. Although the NSANCS design [40] addresses the major limitation of the SANCS array [39] by formulating analytical expressions for element positions and achievable DOF, there is still room for improvement in terms of uDOF and co-array aperture for NCS. Thus, it develops the pursuit of constructing a more robust sparse design for NCS that can provide a larger continuous virtual aperture and enhanced DOF capacity.

Toward this objective, in this paper, we introduce a triad-displaced ULAs (Tdis-ULAs) design for the DOA estimation of NCS. The proposed geometry generally consists of three ULAs, which are appropriately set apart. The Tdis-ULAs structure for NCS possesses all the useful properties, such as a virtual array of larger continuous aperture and a hole-free ULA. Unlike SANCS [39], it uniquely determines the physical sensor locations through analytical expression. While the other parameters for array configuration, including the inter-ULA displacement, the optimal distribution of physical sensors among the ULAs, and the number of uDOF, also benefit from closed-form expressions. More importantly, the proposed configuration offers increased uDOF and wider continuous virtual aperture than NADiS [37], NSANCS [40], and other related sparse arrays. Numerical experiments also validate the performance improvement in comparison with different NULA geometries.

The rest of this paper is organized as follows. In Section 2, the array signal model for NCS is discussed. Section 3 presents the Tdis-ULAs configuration, including its array structure, the achievable DOF, the weight function, and in-built element locations. Section 4 discusses the DOA estimation technique. Simulations are performed in Section 5 to demonstrate the effectiveness of the Tdis-ULAs design. Section 6 concludes this paper.

2. Array signal model

Consider K narrow-band far-field non-circular signals coming from various directions θ_k with corresponding powers $\sigma_k{}^2 (k = 1, 2, \cdots, K)$ incident on an antenna array of N elements, whose fundamental element spacing d in terms of wavelength λ is $d = \lambda/2$. The sensor positions of the array are given by $n_i d$, where n_i (i=1, 2,$\cdots$, N) is in the integer set $P = \{n_1, n_2, \cdots, n_N\}$. Then, the received signal vector for the lth snapshot can be modeled as

$$\boldsymbol{s}(l) = \sum_{k=1}^{K} \boldsymbol{a}(\theta_k) x_k(l) + \boldsymbol{n}(l) = \boldsymbol{A}\boldsymbol{x}(l) + \boldsymbol{n}(l) \tag{1}$$

where $\boldsymbol{x}(l) = [x_1(l), x_2(l), \cdots, x_K(l)]^{\mathrm{T}}$ shows the $K \times 1$ source signal vector. $\boldsymbol{n}(l)$ signifies the additive white Gaussian noise vector with zero mean and variance σ_n^2. $\boldsymbol{A} = [\boldsymbol{a}(\theta_1), \boldsymbol{a}(\theta_2), \cdots, \boldsymbol{a}(\theta_K)]$ is the $N \times K$ array manifold matrix, where $\boldsymbol{a}(\theta_k)$ representing the steering vector for the kth source is given by

$$\boldsymbol{a}(\theta_k) = \left[\begin{array}{c} \mathrm{e}^{-\mathrm{j}2\pi n_1 d \sin\theta_k/\lambda}, \mathrm{e}^{-\mathrm{j}2\pi n_2 d \sin\theta_k/\lambda}, \cdots, \mathrm{e}^{-\mathrm{j}2\pi n_N d \sin\theta_k/\lambda} \end{array} \right]^{\mathrm{T}}. \tag{2}$$

The covariance matrix corresponding to $\boldsymbol{s}(l)$ can be expressed as

$$\boldsymbol{R}_{ss} = \mathrm{E}[\boldsymbol{s}(l)\boldsymbol{s}^{\mathrm{H}}(l)] = \boldsymbol{A}\boldsymbol{R}_{xx}\boldsymbol{A}^{\mathrm{H}} + \sigma_n{}^2\boldsymbol{I} \tag{3}$$

where $\boldsymbol{R}_{xx} = \mathrm{E}[\boldsymbol{x}(l)\boldsymbol{x}^{\mathrm{H}}(l)]$ is the source covariance matrix, and $\boldsymbol{I}$ represents the identity matrix. The correlation between signals observed at the ith and the jth elements can be given as

$$[\boldsymbol{R}_{ss}]_{i,j} = \sum_{k=1}^{K} \mathrm{e}^{-\mathrm{j}2\pi (n_i - n_j) d \sin\theta_k/\lambda} \sigma_k^2 \tag{4}$$

where $n_i, n_j \in P$. Then, the corresponding difference co-array D forming the basis of a virtual array can be defined as

$$D = \{n_i - n_j \mid 1 \leqslant i, j \leqslant N\} \tag{5}$$

where the elements in D are the relative position in the virtual array. Since it is a known fact that the elliptic covariance matrix of NCS has a non-zero value, we have

$$\boldsymbol{R}'_{ss'} = \mathrm{E}[\boldsymbol{s}(l)\boldsymbol{s}^{\mathrm{T}}(l)] \neq 0. \tag{6}$$

This information can be utilized to increase the co-array aperture [39] as

$$\boldsymbol{s}_e(l) = \left[\begin{array}{c} \boldsymbol{s}(l) \\ \boldsymbol{s}^*(l) \end{array} \right] = \left[\begin{array}{c} \boldsymbol{A} \\ \boldsymbol{A}^* \end{array} \right] \boldsymbol{x}(l) + \left[\begin{array}{c} \boldsymbol{n}(l) \\ \boldsymbol{n}^*(l) \end{array} \right], \tag{7}$$

$$\boldsymbol{s}_e(l) = \boldsymbol{B}\boldsymbol{x}(l) + \left[\begin{array}{c} \boldsymbol{n}(l) \\ \boldsymbol{n}^*(l) \end{array} \right], \tag{8}$$

where

$$\boldsymbol{B} = \left[\left(\begin{array}{c} \boldsymbol{a}(\theta_1) \\ \boldsymbol{a}(\theta_1)^* \end{array} \right), \left(\begin{array}{c} \boldsymbol{a}(\theta_2) \\ \boldsymbol{a}(\theta_2)^* \end{array} \right), \cdots, \left(\begin{array}{c} \boldsymbol{a}(\theta_K) \\ \boldsymbol{a}(\theta_K)^* \end{array} \right) \right]$$

denotes the equivalent steering matrix. Then, the extended covariance matrix is given by

$$\boldsymbol{R}_{ss_e} = \mathrm{E}[\boldsymbol{s}_e(l)\boldsymbol{s}_e^{\mathrm{H}}(l)] = \boldsymbol{B}\boldsymbol{R}_{xx}\boldsymbol{B}^{\mathrm{H}} + \sigma_n^2\boldsymbol{I} \tag{9}$$

From the above expression, it is evident that $\boldsymbol{B}\boldsymbol{B}^{\mathrm{H}}$ enlarges the co-array aperture; according to (4), the extended virtual manifold for NCS [39,40] can be expressed as

$$\mathrm{RC}_{\mathrm{NCS}} = \{n_i - n_j, n_i + n_j, -n_i - n_j | 1 \leqslant i, j \leqslant N\}. \tag{10}$$

It is interesting to notice that the extended co-array $\mathrm{RC}_{\mathrm{NCS}}$ for NCS is the combination of difference co-array and sum (with its negative) of co-array. Following (5) and (10), the sum co-array S can be given as

$$S = \{n_i + n_j \mid 1 \leqslant i, j \leqslant N\}. \tag{11}$$

To achieve the maximum uDOF, the number of continuous virtual positions in the extended co-array needs to reach the maximum. Since the utilization of sum and its negative of co-array comes naturally alongside difference co-array when the NCS are considered, all the sparse array configurations throughout this manuscript are evaluated based on extended co-array $\mathrm{RC}_{\mathrm{NCS}}$ [39,40].

3. Tdis-ULAs configuration

This section introduces the Tdis-ULAs geometry for NCS, which effectively concatenates the ULAs to achieve a higher number of uDOF, as displayed in Fig. 1. As the name suggests, the configuration generally consists of three ULAs, with the number of sensors in the ULAs denoted by N_1, N_2, and N_3, respectively. The first N_1-element ULA corresponds to sparse ULA with an inter-sensor spacing of Md, where M is determined by

$$M = 2\lfloor N/4 \rfloor + 2. \tag{12}$$

The sparse ULA is followed by a dense ULA containing N_2 elements with an inter-sensor spacing of d, while the inter-ULA separation between the first two ULAs is set to $Md/2$. The last ULA, which maintains an inter-sensor spacing of d for N_3 elements is further displaced by $2d$, as depicted in Fig. 1. In order to achieve a wider hole-free co-array for Tdis-ULAs array, the sensors must be optimally distributed among the ULAs under the constraint of the total number of sensors, $N = N_1 + N_2 + N_3$. Such an effective distribution of elements is formulated by

$$\begin{cases} N_1 = N - M + 1 \\ N_2 = \dfrac{M}{2} \\ N_3 = \dfrac{M}{2} - 1 \end{cases}. \tag{13}$$

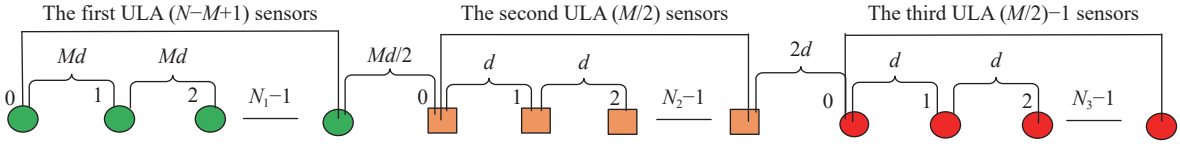

Fig. 1 Proposed Tdis-ULAs configuration

Correspondingly, the set of antenna locations for Tdis-ULAs P_{tdis} is given by

$$\begin{aligned} P_{\mathrm{tdis}} = \Bigg[& \{Mt_1 d \mid t_1 = 0, 1, \cdots, N_1 - 1\} \cup \\ & \left\{\left(\left(N_1 - \frac{1}{2}\right)M + t_2\right)d \mid t_2 = 0, 1, \cdots, N_2 - 1\right\} \cup \\ & \{(N_1 M + 1 + t_3)d \mid t_3 = 0, 1, \cdots, N_3 - 1\}\Bigg]. \end{aligned} \tag{14}$$

3.1 DOF for Tdis-ULAs configuration

It is proposed that the resulting co-array of Tdis-ULAs geometry produces a hole-free virtual ULA denoted by U, i.e., $\mathrm{RC}_{\mathrm{NCS}} = U$. In view of P_{tdis}, the maximum distance between the physical sensors is equal to the distance between the first and the last element, i.e., $N_1 M + M/2 - 1$. Since the resulting co-array for NCS in (10) involves the sum co-array, the maximum distance between the virtual sensors for the positive part of co-array $\mathrm{RC}^{+}_{\mathrm{NCS}}$ is

$$\left(N_1 M + \frac{M}{2} - 1\right) + \left(N_1 M + \frac{M}{2} - 1\right) = 2N_1 M + M - 2.$$

It is noteworthy that the difference co-array is symmetric about origin 0, and the resulting co-array in (10) also consists of the negative of the sum co-array, maintaining symmetric positions with sum co-array about 0 as well. Hence, we are only required to prove that $\mathrm{RC}^{+}_{\mathrm{NCS}}$, obtained from the combination of difference and sum sets, contains a consecutive integer set $\mathbf{Z} = \{1, 2, 3, \cdots, 2N_1 M + M - 2\}$.

Based on the antenna positions set, $P_{\mathrm{tdis}} = \{n_i = 1, 2, \cdots, N\}$, the positive $N-1$ difference sets can be constructed as follows:

$$\begin{cases} D_1 = \{n_2 - n_1, n_3 - n_1, \cdots, n_N - n_1\} \\ D_2 = \{n_3 - n_2, n_4 - n_2, \cdots, n_N - n_2\} \\ \vdots \\ D_{N_1} = \{n_{N_1+1} - n_{N_1}, n_{N_1+2} - n_{N_1}, \cdots, n_N - n_{N_1}\} \\ D_{N_1+1} = \{n_{N_1+2} - n_{N_1+1}, n_{N_1+2} - n_{N_1+1}, \cdots, n_N - n_{N_1+1}\} \\ \vdots \\ D_{N_1+N_2+N_3-2} = D_{N-2} = \{n_{N-1} - n_{N-2}, n_N - n_{N-2}\} \\ D_{N_1+N_2+N_3-1} = D_{N-1} = \{n_N - n_{N-1}\} \end{cases}. \tag{15}$$

Likewise, we may also construct N sum co-arrays as follows:

$$\begin{cases} S_1 = \{n_1 + n_1, n_2 + n_1, \cdots, n_N + n_1\} \\ S_2 = \{n_2 + n_2, n_3 + n_2, \cdots, n_N + n_2\} \\ \vdots \\ S_{N_1} = \{n_{N_1} + n_{N_1}, n_{N_1+1} + n_{N_1}, \cdots, n_N + n_{N_1}\} \\ S_{N_1+1} = \{n_{N_1+1} + n_{N_1+1}, n_{N_1+2} + n_{N_1+1}, \cdots, n_N + n_{N_1+1}\} \\ \vdots \\ S_{N-1} = \{n_{N-1} + n_{N-1}, n_N + n_{N-1}\} \\ S_N = \{n_N + n_N\} \end{cases}. \tag{16}$$

The above difference and sum sets can be concretely expressed as

$$\begin{cases} D_1 = \left\{M, 2M, \cdots, (N_1-1)M, N_1M - \frac{M}{2}, N_1M - \frac{M}{2}+1, \cdots, N_1M-1, N_1M+1, N_1M+2, \cdots, N_1M+\frac{M}{2}-1\right\} \\ D_2 = \left\{M, 2M, \cdots, N_1M-2M, N_1M-\frac{3M}{2}, N_1M-\frac{3M}{2}+1, \cdots, N_1M-M-1, N_1M-M+1, N_1M-M+2, \cdots, N_1M-\frac{M}{2}-1\right\} \\ \vdots \\ D_{N_1-2} = \left\{2M, M, \frac{5M}{2}, \frac{5M}{2}+1, \cdots, 3M-1, 3M+1, 3M+2, \cdots, \frac{7M}{2}-1\right\} \\ D_{N_1-1} = \left\{M, \frac{3M}{2}, \frac{3M}{2}+1, \cdots, 2M-1, 2M+1, 2M+2, \cdots, \frac{5M}{2}-1\right\} \\ D_{N_1} = \left\{\frac{M}{2}, \frac{M}{2}+1 \cdots, M-1, M+1, M+2, \cdots, \frac{3M}{2}-1\right\} \\ D_{N_1+1} = \left\{1, 2, \cdots, \frac{M}{2}-1, \frac{M}{2}+1, \cdots, M-1\right\} \\ \vdots \\ D_{N_1+N_2} = \left\{2, 3, \cdots, \frac{M}{2}\right\} \\ D_{N_1+N_2+1} = \left\{1, 2, \cdots, \frac{M}{2}-2\right\} \\ \vdots \\ D_{N_1+N_2+N_3-1} = D_{N-1} = \{1\} \end{cases}, \quad (17)$$

$$\begin{cases} S_1 = \left\{0, M, \cdots, (N_1-1)M, N_1M - \frac{M}{2}, N_1M - \frac{M}{2}+1, \cdots, N_1M-1, N_1M+1, N_1M+2, \cdots, N_1M+\frac{M}{2}-1\right\} \\ S_2 = \left\{2M, 3M, \cdots, N_1M, N_1M+\frac{M}{2}, N_1M+\frac{M}{2}+1, \cdots, N_1M+M-1, N_1M+M+1, N_1M+M+2, \cdots, N_1M+\frac{3M}{2}-1\right\} \\ S_3 = \left\{4M, 5M, \cdots, N_1M+M, N_1M+\frac{3M}{2}, N_1M+\frac{3M}{2}+1, \cdots, N_1M+2M-1, N_1M+2M+1, N_1M+2M+2, \cdots, N_1M+\frac{5M}{2}-1\right\} \\ \vdots \\ S_{N_1+1} = \left\{2N_1M-M, 2N_1M-M+1, \cdots, 2N_1M-\frac{M}{2}-1, 2N_1M-\frac{M}{2}+1, 2N_1M-\frac{M}{2}+2, \cdots, 2N_1M-M-1\right\} \\ S_{N_1+2} = \left\{2N_1M-M+2, \cdots, 2N_1M-\frac{M}{2}, 2N_1M-\frac{M}{2}+2, 2N_1M-\frac{M}{2}+3, \cdots, 2N_1M\right\} \\ \vdots \\ S_{N_1+N_2} = \left\{2N_1M-2, 2N_1M, 2N_1M+1, \cdots, 2N_1M+\frac{M}{2}-2\right\} \\ S_{N_1+N_2+1} = \left\{2N_1M+2, 2N_1M+3, \cdots, 2N_1M+\frac{M}{2}\right\} \\ \vdots \\ S_{N_1+N_2+N_3} = S_N = \{2N_1M+M-2\} \end{cases}. \quad (18)$$

Let

$$D_0 = D_1 \cup D_2 \cup \cdots \cup D_{N_1} \cup D_{N_1+1} \cup \cdots \cup D_{N-2} \cup D_{N-1}$$

and

$$S_0 = S_1 \cup S_2 \cup \cdots \cup S_{N_1} \cup S_{N_1+1} \cup \cdots \cup S_{N-1} \cup S_N.$$

Then, the proof of $(D_0 \cup S_0) \supset \mathbf{Z}$ can be constituted by finding out the continuous virtual lags $\{tM+1, tM+2, \cdots, (t+1)M\}(0 \leqslant t \leqslant 2N_1)$ from some subsets of $D_0 \cup S_0$. In the first step, the combination of difference sets $D_1 \cup D_{N_1+1} \cup D_{N_1+N_2}$ provides the lag $\{1, 2, \cdots, M\}$. The lag $\{M+1, M+2, \cdots, 2M\}$ can be acquired from the difference sets $D_1 \cup D_{N_1} \cup D_{N_1-1}$. Next, the combination of $D_1 \cup D_{N_1-1} \cup D_{N_1-2}$ can obtain the lag $\{2M+1, 2M+2, \cdots,$

$3M\}$, and so on. Likewise, in an intermediate step, the virtual sensors lag

$$\left\{N_1M-\frac{M}{2}+1, N_1M-\frac{M}{2}+2, \cdots, N_1M+\frac{M}{2}\right\}$$

can be attained from combination of difference and sum sets $D_1 \cup S_2$. Afterward, the combination of different sum co-arrays acquires the remaining virtual lags. The lag

$$\left\{N_1M+\frac{M}{2}+1, N_1M+\frac{M}{2}+2, \cdots, N_1M+\frac{3M}{2}\right\}$$

can be obtained from $S_2 \cup S_3$. Similarly, the combination of $S_3 \cup S_4$ can provide the lag

$$\left\{N_1M+\frac{3M}{2}+1, N_1M+\frac{3M}{2}+2, \cdots, N_1M+\frac{5M}{2}\right\}$$

and so forth.

In the penultimate step, the lag

$$\{2N_1M-M+1, 2N_1M-M+2, \cdots, 2N_1M\}$$

can be obtained from the sets $S_{N_1+1} \cup S_{N_1+2}$. Finally, the combination of the sets $S_{N_1+N_2} \cup S_{N_1+N_2+1} \cup \cdots \cup S_{N-1} \cup S_N$ obtains

$$\{2N_1M-M+1, 2N_1M-M+2, \cdots, 2N_1M\}.$$

Since the integer set $\mathbf{Z}$ consists of the lags $\{tM+1, tM+2, \cdots, (t+1)M\}$, it can be concluded that $(D_0 \cup S_0) \supset \mathbf{Z}$. As $\mathrm{RC}_{\mathrm{NCS}}^{+}$ for the Tdis-ULAs geometry contains distinct elements in $D_0 \cup S_0$, including 0, we can derive $\mathrm{RC}_{\mathrm{NCS}}^{+} \supset \mathbf{Z}$. Recall that (10) consists of three co-arrays; a difference co-array is symmetrical about 0, while the sum (with its negative) of co-array also develops a set of symmetric positions about 0. Subsequently, the resulting co-array constitutes the symmetric set of the hole-free virtual positions about 0, i.e., $\{-(2N_1M+M-2), -(2N_1M+M-2)+1, \cdots, -2, -1, 0, 1, 2, \cdots, 2N_1M+M-2\}$. Therefore, it concludes that the extended co-array of the Tdis-ULAs design is a hole-free ULA U for which the corresponding uDOF can be determined as

$$\mathrm{uDOF} \approx N^2+3N-7. \tag{19}$$

Substitute expressions of N_1 and M in (19), and

$$\mathrm{uDOF} = 8N\left\lfloor\frac{N}{4}\right\rfloor - 16\left\lfloor\frac{N}{4}\right\rfloor^2 - 20\left\lfloor\frac{N}{4}\right\rfloor + 8N - 7. \tag{20}$$

The above formula can be approximately expressed by using $N/4$ instead of $\lfloor N/4 \rfloor$. Therefore, the uDOF can be calculated by

$$\mathrm{uDOF} \approx N^2+3N-7. \tag{21}$$

Note the above approximation is accurate for all the even integers satisfying $N\%4 = 0$, with $\%$ showing the remainder. For other integers, the difference between approximate and true uDOF is between 4 and 6. Specifically, the uDOF can be obtained by

$$\mathrm{uDOF} = \begin{cases} N^2+3N-7, & N\%4=0 \\ N^2+3N-3, & N\%4=1 \\ N^2+3N-1, & \text{otherwise} \end{cases}. \tag{22}$$

It is to be noted that the Tdis-ULAs design realizes a hole-free resulting co-array with any number of sensors, except for $N = 5$, $N = 6$, and $N = 7$. Thus, the $\mathrm{uDOF}_{\mathrm{tdis}}$ denoting the achievable DOF for the Tdis-ULAs can be accurately calculated by

$$\mathrm{uDOF}_{\mathrm{tdis}} = \mathrm{uDOF} - 4a \tag{23}$$

where a assumes the values 0 and 1 to provide the corresponding uDOF as given below:

$$\begin{cases} a=1, & N=5; N=6; N=7 \\ a=0, & \text{otherwise} \end{cases}. \tag{24}$$

For an illustrative comparison of uDOF and continuous virtual aperture, Fig. 2 shows the 11-element structure of Tdis-ULAs and other NULA designs using the same number of sensors with an extended co-array aperture for NCS [39,40]. It can be easily observed in Fig. 2 that only the proposed array and the NSANCS [40] array produce a hole-free resulting ULA. Importantly, the Tdis-ULAs configuration achieves the highest number of continuous virtual positions and the largest continuous virtual aperture among all the other antenna arrays.

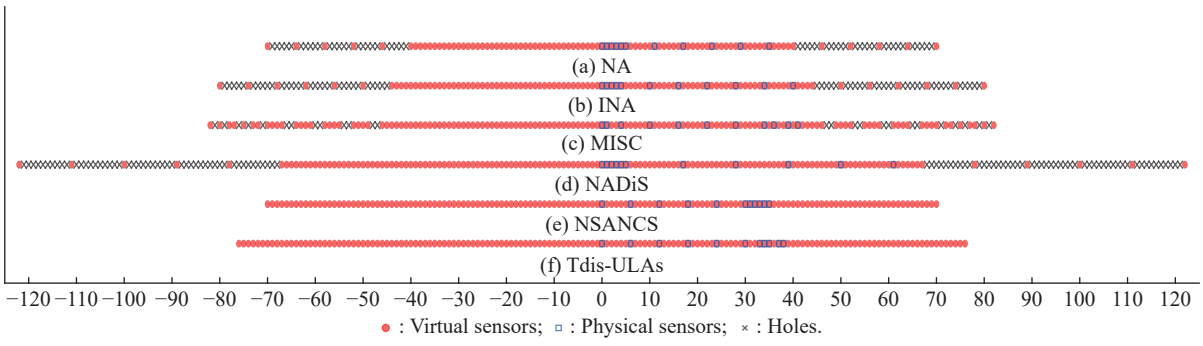

Fig. 2 Geometric distribution of physical sensors and virtual sensors of eleven-element array configurations

Remark 1 A noticeable fact from Fig. 2 is that the proposed configuration occupies the physical space (coverage with physical sensors) much lower than that of INA [22], MISC [30], and NADiS [37] configurations. Advantageously, its continuous virtual aperture, which is crucial for improving the DOA estimation accuracy, is significantly larger than all the other configurations, followed by NSANCS [40] and NADiS [37]. Although the Tdis-ULAs design has a marginally larger physical aperture than NSANCS [40], its hole-free co-array property makes the proper and effective use of this since it improves the continuous virtual aperture by four times against this increase in the physical aperture, which is quite remarkable. In particular, the continuous virtual aperture of Tdis-ULAs using eleven sensors is 152, which is approximately 9% wider than that of NSANCS [40] with the same number of sensors, and compared to the NADiS [37], it increases the continuous virtual aperture by almost 17%. On the contrary, the NADiS [37], MISC [30], and INA [22] consume more physical space, but their resulting co-array suffers from holes, which eventually restricts the effective use of their virtual aperture.

Furthermore, Table 1 lists the uDOF offered by sparse array configurations for NCS over a varying number of elements. The NNA [38] and SANC [39] not worked out for certain N are marked as "N/A". It is observed that the NA [18] has the lowest uDOF capacity, followed by INA [22] and MISC [30]. In comparison, the NSACNS [40] achieves more uDOF than the NA [18], INA [22], MISC [30], and NADiS [37] arrays. Advantageously, the Tdis-ULAs geometry obtains the maximum number of uDOF and thus outperforms all the sparse arrays in the data comparison Table 1. Besides, this enhancement in uDOF gets more evident as the element number increases further.

Table 1 Comparison of achievable DOF

Array configuration	Number of sensors N							
	7	9	10	11	13	14	17	21
NA	37	57	69	81	109	125	177	261
INA	43	65	77	91	121	137	193	281
NSANCS	61	97	117	141	193	221	321	481
MISC	43	69	81	93	129	145	201	297
SANC	65	105	129	N/A	N/A	N/A	N/A	N/A
NNA	N/A	N/A	93	N/A	N/A	211	N/A	N/A
NADiS	55	89	109	131	181	209	305	461
Proposed array	65	105	129	153	205	237	339	501

Remark 2 It is witnessed in Table 1 that the number of DOF obtained by NADiS [37] using eleven sensors is almost equal to that obtained by the proposed configuration using only ten sensors. In comparison, the MISC [30] requires thirteen sensors to achieve the same number of DOF, followed by INA [22] and NA [18], which would need an even higher number of sensors to achieve this DOF capacity. Thus, these configurations can offer relatively similar performance as Tdis-ULAs but only at the expense of additional sensor(s), which eventually leads to more hardware costs and complexities. Hence, the proposed sparse array is more suitable for many applications, including under-determined systems, where it is imperative to handle more sources at a lower expense of resources.

Next, we present a discussion on mutual coupling effects between array sensors, which is significant in the practical environment. The role of weight function $w(g)$, which indicates the number of sensor pairs with an inter-sensor spacing of g, is vital for quantifying the mutual coupling effect in sensor arrays [30]. The weight functions at smaller separation, mainly the first three, i.e., $w(1)$, $w(2)$, and $w(3)$, are known to be the key to gauging mutual coupling effects, with the first weight function having the highest impact, followed by the second [30]. The smaller the value of these weight functions, the lower the coupling effects [30].

In this regard, we evaluate the weight functions of different sensor array configurations in Fig. 3, where N = 11. It can be observed that NA [18] and INA [22] have the first three weight function values of 5, 4, 3 and 4, 3, 2, respectively. In comparison, the proposed sparse array is less affected by the mutual coupling effects as it owns smaller weight function values of 3, 2, and 3. Although the MISC array [30], originally designed for the CS, has the corresponding values of 1, 2, and 2, with the lowest value for the first weight function, its value for the second weight function is the same as that of Tdis-ULAs. Knowing from earlier results, the Tdis-ULAs have considerable benefits over MISC arrays [30], such as a DOF capacity almost 65% higher, a continuous virtual aperture 66% larger, consuming lower physical space, requiring fewer physical sensors, and advantageously a hole-free resulting co-array, making it quite versatile in overall advantages.

Moreover, the comparison of the proposed sparse array with its related counterpart configurations for NCS is worth noticing. It can be observed that the weight function values of NSANCS [40] and NADiS [37] configurations are identical, with the value of their first three weight functions being 5, 4, and 3, respectively. Therefore, compared to NADiS [37] and NSANCS [40], the proposed sparse array is more robust since it owns

smaller weight function values and thus can greatly reduce the mutual coupling effects. Besides, it also offers other benefits, including higher DOF capacity and a larger continuous virtual aperture. Meanwhile, the other advantage of Tdis-ULAs is to provide in-built physical locations so that the extension of the proposed array to a larger aperture can be relatively easier, as further discussed in the following subsection.

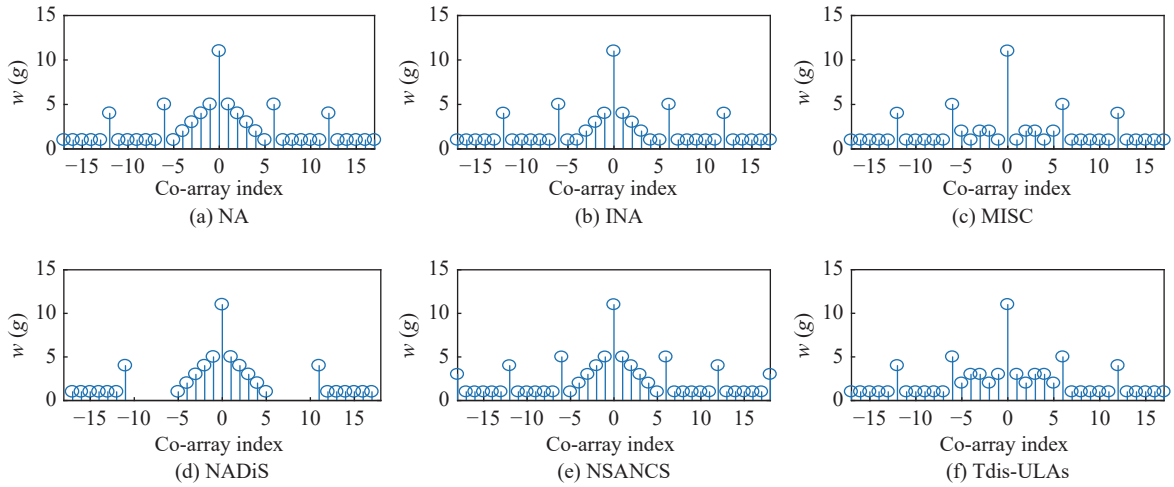

Fig. 3 Weight functions of six eleven-element array configurations

3.2 In-built element locations

The proposed configuration can also provide in-built physical locations for the Tdis-ULAs structures constructed in a range of elements that satisfies the given conditions. In particular, the proposed Tdis-ULAs design maintains $M-3$ identical antenna positions for the Tdis-ULAs structures designed in an interval, where the initial element N_i satisfies $N\%4=0$, while the last element N_l in the quaternate interval follows $N\%4=3$.

Under the given conditions, consider a range of four consecutive elements, such as elements in the interval [12,15], i.e., $N_i=12\%4=0$, $N_l=15\%4=3$. The value of $M=8$ can be obtained from (12). Here, designing the proposed Tdis-ULAs structure for $N=12$ will automatically provide the first $M-3$ physical locations of its array design for $N=13$, $N=14$, and $N=15$. Fig. 4 displays the geometric configurations of Tdis-ULAs for the elements in this interval. It can be seen that all the Tdis-ULAs structures in this interval possess identical $M-3$ physical locations. Hence the construction of the proposed Tdis-ULAs geometry for any of these elements advantageously reveals $M-3$ locations for designing the remaining Tdis-ULAs structures in this range. Thus, extending and maneuvering the Tdis-ULAs array to a larger aperture within this interval is relatively easier, which is an added advantage of the proposed sparse array.

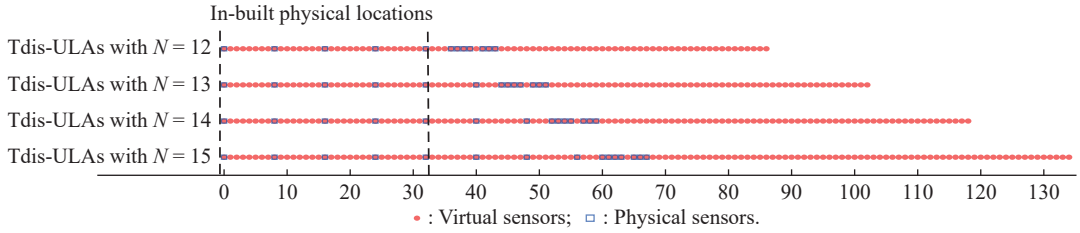

Fig. 4 Distribution of physical sensors and virtual sensors of Tdis-ULAs for four consecutive elements

Remark 3 The desirable characteristics of the proposed antenna array approach for NCS are summarized as follows:

(i) Due to the availability of closed-form expressions array design and uDOF, the proposed configuration is systematically constructed.

(ii) The extended resulting co-array of the Tdis-ULAs structure is also a filled ULA.

(iii) Compared to its sparse counterpart arrays, the Tdis-ULAs geometry achieves maximum uDOF and a larger

continuous virtual aperture for the same number of elements.

(iv) Advantageously, the Tdis-ULAs provide in-built element positions in a given interval of physical sensors.

4. DOA estimation

In this section, we discuss the spatial smoothing technique for performing the DOA estimation. To fully exploit the maximum continuous virtual array, we vectorized the extended covariance matrix $\boldsymbol{R}_{ss_e}$ in (9) [39] as

$$z = \mathrm{vec}(\boldsymbol{R}_{ss_e}) = \mathrm{vec}\left[\sum_{k=1}^{K}\sigma_k^2\boldsymbol{b}(\theta_k)\boldsymbol{b}(\theta_k)^{\mathrm{H}} + \sigma_n^2\boldsymbol{I}\right] = \boldsymbol{C}\boldsymbol{p}_k + \sigma_n^2\breve{1}_n \tag{25}$$

where $\boldsymbol{C} = [\boldsymbol{c}(\theta_1), \boldsymbol{c}(\theta_2), \cdots, \boldsymbol{c}(\theta_K)]$ signifies the extended virtual array manifold, with $\boldsymbol{c}(\theta_k) = \boldsymbol{b}^*(\theta_k) \otimes \boldsymbol{b}(\theta_k)$ (k = 1, 2, $\cdots$, K), and $\boldsymbol{p}_k = [{\sigma_1}^2, {\sigma_2}^2, \cdots, {\sigma_K}^2]^{\mathrm{T}}$. Since the extended co-array is symmetric about 0, we set the total number of consecutive virtual sensors as $2L_c$+1, indicating that the virtual locations are continuous in $[-L_c, L_c]$. As $\boldsymbol{z}$ is a single snapshot in the virtual array, we need to apply the spatial smoothing method in order to work with the multiple signal classification (MUSIC) technique for estimating multiple sources [18,39]. Because the spatial smoothing technique uses the range of consecutive virtual sensors [18,39], we take the maximum continuous response segment in $\boldsymbol{C}$ to reconstruct a new $z_e \in \mathbf{C}^{(2L_c+1)\times 1}$ vector as

$$z_e = \boldsymbol{C}_n\boldsymbol{p}_k + \sigma_n^2\breve{1}_n \tag{26}$$

where $\boldsymbol{C}_n$ denotes the virtual array manifold for a range of continuous virtual locations. The spatial smoothing is then applied to vector $\boldsymbol{z}_e$, which holds conjugate symmetric distribution. Thus, the length of the smooth segment is $L_{ss} = L_c$+1. The sensor locations for the ith smooth subarray $\breve{z}_i$ are given as

$$\{(-i+1+n)d, n = 0, 1, \cdots, L_c\}$$

and $\breve{z}_i$ can be shown as

$$\breve{z}_i = \breve{\boldsymbol{C}}_i p_k + {\sigma_n}^2\breve{1}_i = \breve{\boldsymbol{C}}_i\boldsymbol{\Phi}^{i-1}\boldsymbol{p}_k + {\sigma_n}^2\breve{1}_i$$

where

$$\boldsymbol{\Phi} = \begin{pmatrix} \mathrm{e}^{-\mathrm{j}\pi\sin\theta_1} & & & \\ & \mathrm{e}^{-\mathrm{j}\pi\sin\theta_2} & & \\ & & \ddots & \\ & & & \mathrm{e}^{-\mathrm{j}\pi\sin\theta_K} \end{pmatrix}, \tag{27}$$

$$\breve{\boldsymbol{C}}_1 = \begin{pmatrix} 1 & 1 & \cdots & 1 \\ \breve{c}(\theta_1) & \breve{c}(\theta_2) & \cdots & \breve{c}(\theta_K) \\ \vdots & \vdots & \ddots & \vdots \\ \breve{c}(\theta_1)^{L_c} & \breve{c}(\theta_2)^{L_c} & \cdots & \breve{c}(\theta_K)^{L_c} \end{pmatrix}, \tag{28}$$

$$\breve{\boldsymbol{c}}(\theta_i) = \left[1, \breve{c}(\theta_i), \cdots, \breve{c}(\theta_i)^{L_c}\right]^{\mathrm{T}}, \tag{29}$$

$$\breve{c}(\theta_i) = \mathrm{e}^{-\mathrm{j}\pi\sin\theta_i}. \tag{30}$$

Now we take the average of all covariance matrices of smooth subarrays for obtaining a spatially smooth matrix $\boldsymbol{R}_{\mathrm{SM}}$ [39] given as

$$\boldsymbol{R}_{\mathrm{SM}} = \frac{1}{L_{ss}}\sum_{i=1}^{L_{ss}}\breve{\boldsymbol{z}}_i\breve{\boldsymbol{z}}_{ii}^{\mathrm{H}}. \tag{31}$$

The MUSIC algorithm can then be successfully applied to $\boldsymbol{R}_{\mathrm{SM}}$ for estimating the DOA of multiple incoming sources. This use of spatial smoothing with the MUSIC algorithm is commonly referred to as the spatial smoothing MUSIC (SS-MUSIC) method [18,39].

5. Simulation results

One of the key features of NULA configurations is their ability to estimate DOAs in under-determined conditions. This section conducts different experimental works to show that the Tdis-ULAs structure retains this advantage while demonstrating its superiority over other sparse arrays. It is worth mentioning that for a fair comparison, all the array configurations in the simulation section are evaluated with an extended co-array for NCS [39,40]. Moreover, to perform the DOA estimation and evaluate the simulation results, we have employed the SS-MUSIC method [18,39]. Firstly, the spatial spectrum of SS-MUSIC of the sparse arrays is compared, where the DOAs of multiple sources are estimated in an under-determined scenario. Next, we examine the uDOF capacity of sparse arrays in terms of the number of sensors, as suggested in [22]. Later, using the SS-MUSIC method, we study the DOA estimation performance of these sparse arrays through Monte Carlo simulations. In particular, we employ root mean square error (RMSE), widely adopted as the performance metric [18,39,40], to estimate the DOAs in terms of signal to noise ratio (SNR) and the number of snapshots. Finally, the comparison of resolution ability is drawn.

5.1 Spatial spectrum analysis

In the first simulation, we compare the ability of Tdis-ULAs design with other geometries to detect and resolve more sources than the physical sensors. For the perfor-

mance analysis, we consider four NULAs, NA [18], INA [22], NSANCS [40], and the proposed sparse array, with $N = 11$ elements, on which $K = 36$ binary phase shift keying (BPSK) signals impinge with equal power. The number of snapshots is set to 250 for a 0 dB SNR. Fig. 5 depicts the DOAs estimated by these sparse arrays, where the sources are uniformly distributed between -50° and 50°. Due to the lower DOF capacity of the NA [18] and INA [22], they fail to estimate the DOAs accurately, and their spatial spectrum is of lower quality compared to the other two counterpart arrays in Fig. 5. While the NSANCS array [40], which possesses comparatively higher DOF, detects the sources more correctly than [18,22]. It can be easily observed that in comparison with all these configurations, the proposed array most accurately estimates the DOAs of all the sources. Hence, it retains the key benefit of employing sparse arrays in under-determined conditions, i.e., $K > N$.

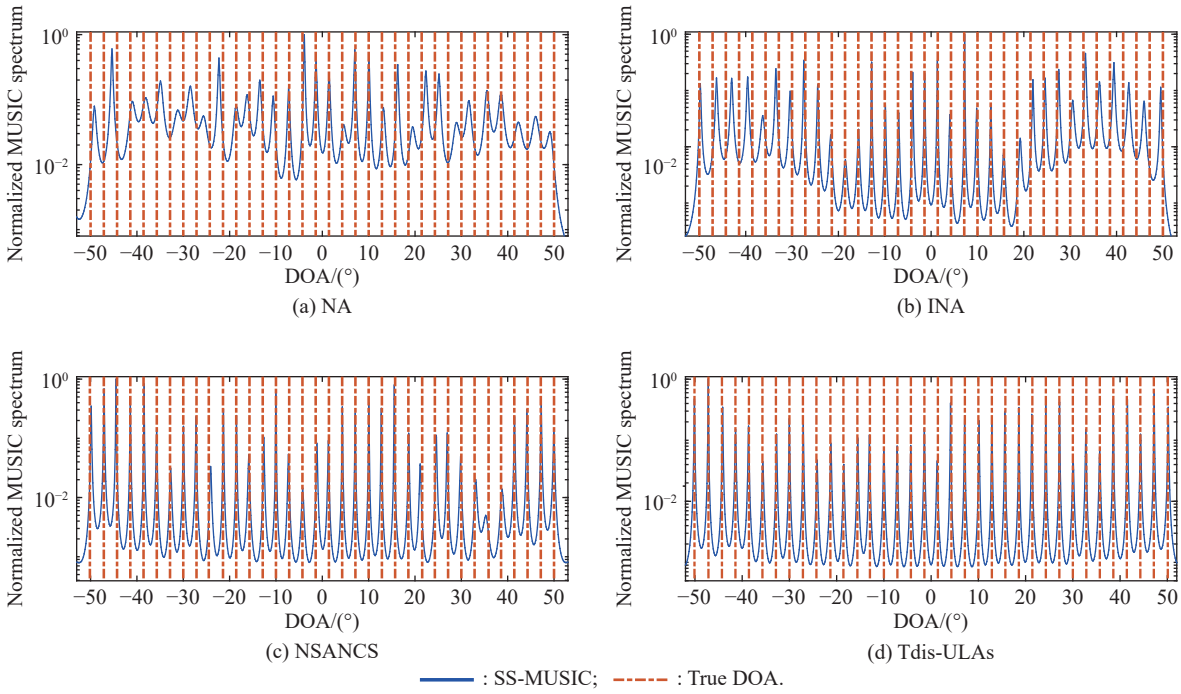

Fig. 5 MUSIC spectra of four eleven-element array configurations

5.2 DOF versus number of sensors

This numerical work evaluates and compares the DOF capacity versus the number of sensors of Tdis-ULAs configuration with other sparse arrays [18,22,30,37,40]. Fig. 6 displays these results. It is easy to observe in Fig. 6 that the proposed design has the highest DOF capacity, followed by NSANCS [40] and NADiS [37]. While the other configurations, NA [18], INA [22], and MISC [30], have failed to offer significant improvements due to their structural limitation when it comes to utilizing the non-circular characteristics or the extended co-array effectively. On the other hand, the DOF improvement shown by the Tdis-ULAs becomes more significant as the number of elements increases, which is truly desirable.

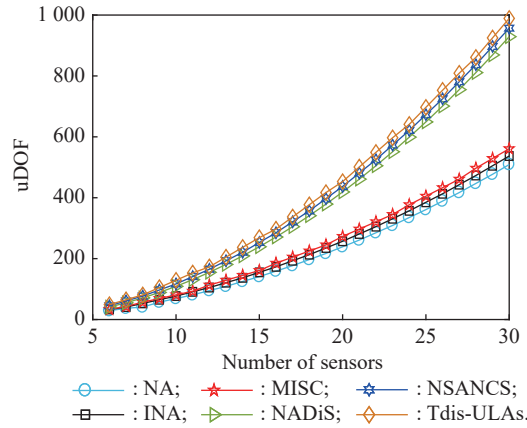

Fig. 6 Achievable DOF versus number of sensors for typical NULA configurations

5.3 RMSE performance

In this experimental part, we demonstrate the DOA esti-

mation performance of the NULA configurations, NA [18], INA [22], MISC [30], NADiS [37], NSANCS [40], and the proposed array via the RMSE [30,40], which can be defined as

$$\text{RMSE} = \sqrt{\frac{1}{500K}\sum_{i=1}^{500}\sum_{k=1}^{K}\left(\hat{\theta}_{i,k}-\theta_k\right)^2} \tag{32}$$

where $\hat{\theta}_{i,k}$ is the estimation of θ_k in the ith $(i=1,2,\cdots,500)$ trial.

Now we evaluate the DOA estimation accuracy in terms of SNR first, for which eleven elements are used for each sparse array configuration. For this experimental setup, we assume N = 13 sources, uniformly distributed in $[-55°, 55°]$, incident on these arrays with the number of snapshots is kept to 200 for a wide range of varying SNR, [−5:2.5:12.5] dB. Fig. 7 plots the corresponding measurement of RMSE as a function of SNR. Simulation results show that the Tdis-ULAs design has a lower RMSE curve over the increasing range of SNR than all other arrays, reflecting its superior DOA estimation performance.

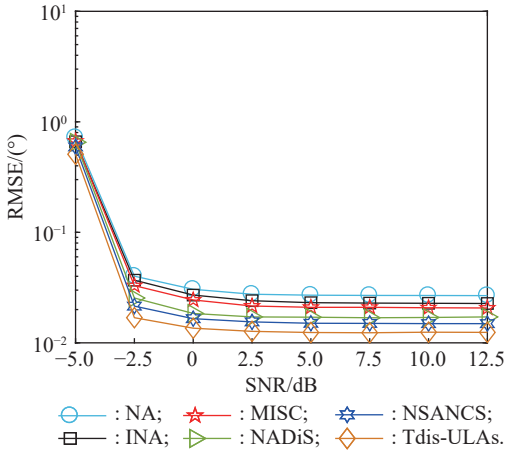

Fig. 7 RMSE versus SNR for typical NULA configurations

The number of snapshots is another critical factor for examining DOA estimation performance of sparse arrays [40]. To evaluate this, we consider the same parameters as in the last experimental work, except the 0 dB fixed SNR over a varying range of snapshots. Fig. 8 depicts the simulation results. It can be observed from Fig. 8 that as the number of snapshots increases, RMSE value tends to decrease for sparse arrays. Noticeably, when the number of snapshots is greater than 90, the Tdis-ULAs array achieves a lower RMSE value than all other sparse arrays. Moreover, it is observed that the RMSE value of NSANCS [40] by consuming 1 050 snapshots is almost equal to that of the proposed array using only 700 samples. Thus, the Tdis-ULAs design requires fewer snapshots, i.e., saving almost 34% samples, to yield the same performance as NSANCS [40], which is remarkable.

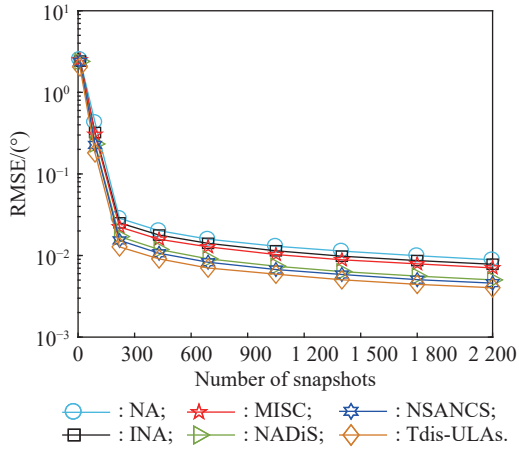

Fig. 8 RMSE versus number of snapshots for typical NULA configurations

5.4 Resolution ability

In this simulation example, we illustrate the resolution performance of different arrays by considering two sources located closely at $\theta_1 = 50°, \theta_2 = 50.7°$, and then evaluating their SS-MUSIC spatial spectrum to check if these arrays can accurately resolve the two sources. Fig. 9 shows the SS-MUSIC spectrum of NA [18], INA [22], MISC [30], NADiS [37], NSANCS [40], and the proposed sparse array, where the number of snapshots and SNR are set to 200 and 0 dB, respectively. Due to increased uDOF, the proposed configuration, NSANCS [40] and NADiS [37], can resolve the DOA of two closely-spaced sources successfully, while NA [18], INA [22], and MISC [30] arrays are unable to separate the targets. Also, benefiting from a larger continuous virtual aperture and higher uDOF, the Tdis-ULAs array correctly identifies both sources and performs more accurately than NADiS [37] and NSANCS [40].

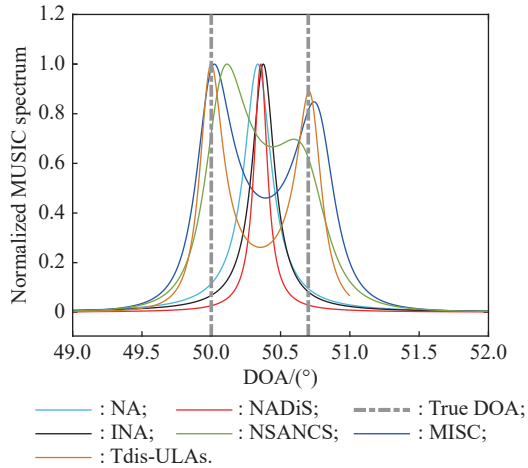

Fig. 9 Spatial spectrum of typical NULA configurations for two closely spaced targets

6. Conclusions

This paper proposes a Tdis-ULAs configuration for NCS that achieves an enhanced DOA estimation accuracy. The configuration appropriately places three ULAs for effective utilization of the non-circular characteristics of the sources. The Tdis-ULAs design offers higher uDOF and wider continuous co-array aperture than its other sparse counterpart arrays. Besides, it produces a hole-free resulting co-array. Moreover, the proposed approach benefits from the closed-form expressions for the array configuration and the number of uDOF. The simulation results also confirm the performance superiority of the proposed configuration.

References

[1] WAN L T, HAN G J, SHU L, et al. The application of DOA estimation approach in patient tracking systems with high patient density. IEEE Trans. on Industrial Informatics, 2016, 12(6): 2353–2364.

[2] QIN Y H, LIU Y M, LIU J Y, et al. Underdetermined wideband DOA estimation for off-grid sources with coprime array using sparse bayesian learning. Sensors, 2018, 18(1): 253.

[3] SHAIKH A H, DANG X Y, AHMED T, et al. New transmit-receive array configurations for the MIMO radar with enhanced degrees of freedom. IEEE Communications Letters, 2020, 24(7): 1534–1538.

[4] SHAIKH A H, DANG X Y, HUANG D Q. New generalized multi-structured mimo radar configuration with increased degrees of freedom. IEEE Communications Letters, 2021, 25(4): 1293–1297.

[5] SHAN T J, WAX M, KAILATH T. On spatial smoothing for direction-of-arrival estimation of coherent signals. IEEE Trans. on Acoustics Speech and Signal Processing, 1985, 33(4): 806–811.

[6] ROY R, KAILATH T. ESPRIT-estimation of signal parameters via rotational invariance techniques. IEEE Trans. on Acoustics Speech and Signal Processing, 1989, 37(7): 984–995.

[7] LI J F, JIANG D F, ZHANG X F. DOA estimation based on combined unitary ESPRIT for coprime MIMO radar. IEEE Communications Letters, 2017, 21(1): 96–99.

[8] ZHENG Z, HUANG Y X, WANG W Q, et al. Augmented covariance matrix reconstruction for DOA estimation using difference coarray. IEEE Trans. on Signal Processing, 2021, 69: 5345–5358.

[9] HE Z Q, SHI Z P, HUANG L, et al. Underdetermined DOA estimation for wideband signals using robust sparse covariance fitting. IEEE Signal Processing Letters, 2015, 22(4): 435–439.

[10] MA W K, HSIEH T H, CHI C Y. DOA estimation of quasi-stationary signals with less sensors than sources and unknown spatial noise covariance: a Khatri-Rao subspace approach. IEEE Trans. on Signal Processing, 2010, 58(4): 2168–2180.

[11] AHMED A, ZHANG Y D. Generalized non-redundant sparse array designs. IEEE Trans. on Signal Processing, 2021, 69: 4580–4594.

[12] HOCTOR R T, KASSAM S A. The unifying role of the coarray in aperture synthesis for coherent and incoherent imaging. Proceedings of the IEEE, 1990, 78(4): 735–752.

[13] BOUDAHER E, AHMAD F, AMIN M G, et al. Mutual coupling effect and compensation in non-uniform arrays for direction-of-arrival estimation. Digital Signal Processing, 2017, 61(2): 3–14.

[14] MOFFET A. Minimum-redundancy linear arrays. IEEE Trans. on Antennas and Propagation, 1968, 16(2): 172–175.

[15] ISHIGURO M. Minimum redundancy linear arrays for a large number of antennas. Radio Science, 1980, 15(6): 1163–1170.

[16] LINEBARGER D A, SUDBOROUGH I H, TOLLIS I G. Difference bases and sparse sensor arrays. IEEE Trans. on Information Theory, 1993, 39(2): 716–721.

[17] PAL P, VAIDYANATHAN P P. Multiple level nested array: an efficient geometry for 2qth order cumulant based array processing. IEEE Trans. on Signal Processing, 2012, 60(3): 1253–1269.

[18] PAL P, VAIDYANATHAN P P. Nested arrays: a novel approach to array processing with enhanced degrees of freedom. IEEE Trans. on Signal Processing, 2010, 58(8): 4167–4181.

[19] VAIDYANATHAN P P, PAL P. Sparse sensing with co-prime samplers and arrays. IEEE Trans. on Signal Processing, 2011, 59(2): 573–586.

[20] QIN S, ZHANG Y D, AMIN M G. Generalized coprime array configurations for direction-of-arrival estimation. IEEE Trans. on Signal Processing, 2015, 63(6): 1377–1390.

[21] LIU C L, VAIDYANATHAN P P. Super nested arrays: linear sparse arrays with reduced mutual coupling—part I: fundamentals. IEEE Trans. on Signal Processing, 2016, 64(15): 3997–4012.

[22] YANG M L, SUN L, YUAN X, et al. Improved nested array with hole-free DCA and more degrees of freedom. Electronics Letters, 2016, 52(25): 2068–2070.

[23] ZHENG Z, YANG C L, WANG W Q, et al. Robust DOA estimation against mutual coupling with nested array. IEEE Signal Processing Letters, 2020, 27: 1360–1364.

[24] LIU J Y, ZHANG Y M, LU Y L, et al. Augmented nested arrays with enhanced DOF and reduced mutual coupling. IEEE Trans. on Signal Processing, 2017, 65(21): 5549–5563.

[25] ZHAO P J, HU G B, QU Z Y, et al. Enhanced nested array configuration with hole-free co-array and increasing degrees of freedom for DOA estimation. IEEE Communications Letters, 2019, 23(12): 2224–2228.

[26] PAL P, VAIDYANATHAN P P. Coprime sampling and the music algorithm. Proc. of the Digital Signal Processing and Signal Processing Education Meeting, 2011: 289–294.

[27] ZHOU C W, GU Y J, FAN X, et al. Direction-of-arrival estimation for coprime array via virtual array interpolation. IEEE Trans. on Signal Processing, 2018, 66(22): 5956–5971.

[28] YADAV S K, GEORGE N V. Fast direction-of-arrival estimation via coarray interpolation based on truncated nuclear norm regularization. IEEE Trans. on Circuits and Systems II: Express Briefs, 2020, 68(4): 1522–1526.

[29] MAHMUD T H A, SHABIR K, ZHENG R, et al. Interpolating coprime arrays with translocated and axis rotated compressed subarrays by iterative power factorization for DOA estimation. IEEE Access, 2018, 6: 16445–16453.

[30] ZHENG Z, WANG W Q, KONG Y, et al. MISC array: a new sparse array design achieving increased degrees of freedom and reduced mutual coupling effect. IEEE Trans. on Signal Processing, 2019, 67(7): 1728–1741.

[31] SHAIKH A H, DANG X Y, KHOSO I A, et al. Three-stage

padding configuration for sparse arrays with larger continuous virtual aperture and increased degrees of freedom. IEICE Trans. on Fundamentals of Electronics, Communications and Computer Sciences, 2022, E105-A(3): 549–561.

[32] SHAIKH A H, DANG X Y, HUANG D Q. A pentad-displaced ULAs configuration with hole-free co-array and increased degrees of freedom for direction of arrival estimation. Digital Signal Processing, 2021, 118(11): 103243.

[33] WAN L T, LIU K H, LIANG Y C, et al. DOA and polarization estimation for non-circular signals in 3-D millimeter wave polarized massive MIMO systems. IEEE Trans. on Wireless Communications, 2021, 20(5): 3152–3167.

[34] GOWRI K, PALANISAMY P, AMIRI I S. Improved method of direction finding for non circular signals with wavelet denoising using three parallel uniform linear arrays. Wireless Personal Communications, 2020, 115(1): 291–305.

[35] TENG L P, WANG Q, CHEN H. 1-Bit DOA estimation algorithm for strictly non-circular sources. IEEE Communications Letters, 2021, 25 (7): 2216−2220.

[36] CAI J J, LIU W, ZONG R, et al. Sparse array extension for non-circular signals with subspace and compressive sensing based DOA estimation methods. Signal Processing, 2018, 145(4): 59–67.

[37] GUPTA P, AGRAWAL M. Design and analysis of the sparse array for doa estimation of noncircular signals. IEEE Trans. on Signal Processing, 2019, 67(2): 460–473.

[38] IWAZAKI S, ICHIGE K. Underdetermined direction of arrival estimation by sum and difference composite co-array. Proc. of the IEEE 25th International Conference on Electronics, Circuits and Systems, 2018: 669–672.

[39] ZHANG Y K, XU H Y, WANG D M, et al. A novel designed sparse array for noncircular sources with high degree of freedom. Mathematical Problems in Engineering, 2019: 1264715.

[40] SHAIKH A H, DANG X Y, KHOSO I A, et al. New sparse array for non-circular sources with increased degrees of freedom. Electronics Letters, 2021, 57(8): 339–342.

Biographies

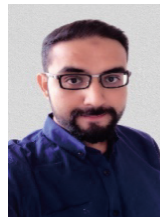

SHAIKH Abdul Hayee was born in 1990. He received his M.E. degree in computer and information engineering in 2016. He is currently working toward his Ph.D. degree in communication and information systems at Nanjing University of Aeronautics and Astronautics. His research interests include array signal processing and wireless communications technology.

E-mail: shaikhhayee@yahoo.com

DANG Xiaoyu was born in 1973. He received his Ph.D. degree from Brigham Young University, Provo, UT, USA, in 2009. Then, he joined College of Electronic and Information Engineering, Nanjing University of Aeronautics and Astronautics. He has received more than 10 research grants from the National Natural Science Foundation of China and other central government agencies. His research interests include wireless network and signal processing with application to aeronautical and astronautical communications.

E-mail: dang@nuaa.edu.cn

HUANG Daqing was born in 1959. He is with the College of Electronics and Information Engineering, Nanjing University of Aeronautics and Astronautics. His research interests include telemetry of UAVs and other related telecommunication systems.

E-mail: 857337053@qq.com